

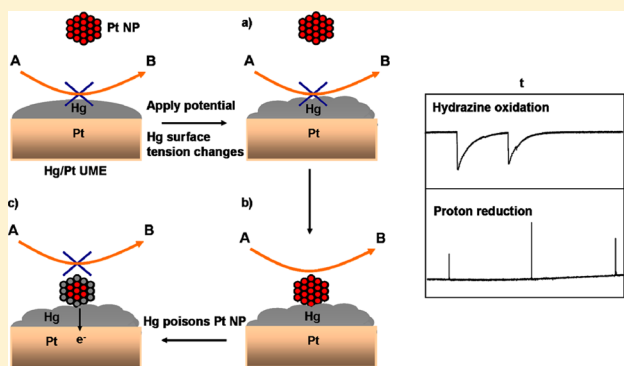
## Influence of the Redox Indicator Reaction on Single-Nanoparticle Collisions at Mercury- and Bismuth-Modified Pt Ultramicroelectrodes

Radhika Dasari, Brandon Walther, Donald A. Robinson, and Keith J. Stevenson\*

Department of Chemistry, The University of Texas at Austin, 1 University Station, Austin, Texas 78712, United States

## Supporting Information

**ABSTRACT:** Single-Pt nanoparticles (NPs) can be detected electrochemically by measuring the current–time ( $i-t$ ) response associated with both hydrazine oxidation and proton reduction during individual Pt NP collisions with noncatalytic Hg- and Bi-modified Pt ultramicroelectrodes (Hg/Pt and Bi/Pt UMEs, respectively). At Hg/Pt UMEs, the  $i-t$  response for both hydrazine oxidation and proton reduction consists of repeated current “spikes” that return to the background level as Hg poisons the Pt NP after collision with the Hg/Pt UME due to amalgamation and deactivation of the redox reaction. Furthermore, at a Hg/Pt UME, the applied potential directly influences the interfacial surface tension (electrocapillarity) that also impacts the observed  $i-t$  response for single-Pt NP collisions for proton reduction that exhibits a faster decay of current (0.7–4 ms) to background levels than hydrazine oxidation (2–5 s). Because the surface tension of Hg is lower (−0.9 V), Pt NPs possibly react faster with Hg (amalgamate at a faster rate), resulting in sharp current spikes for proton reduction compared to hydrazine oxidation. In contrast, a stepwise “staircase”  $i-t$  response is observed for proton reduction for single-Pt NP collisions at a Bi/Pt UME. This different response suggests that electrostatic forces of negatively charged citrate-capped Pt NPs also influence the  $i-t$  response at more negative applied potentials, but the Pt NPs do not poison the electrochemical activity at Bi/Pt UMEs.



## INTRODUCTION

Electrochemical approaches describing observation of single-nanoparticle (NP) collision events with an electrode surface are of immense importance. These studies not only aid in understanding the dynamic behavior of particles diffusing to the electrode surface but also facilitate high-throughput screening of the NP catalytic activity ideally at the single-NP level. These experiments in turn allow the precise correlation of structure–function relationships of NPs and establish new analytical methods for identifying new catalysts.

Various strategies for detecting particle–electrode collisions by measuring non-faradaic charge transfer during a particle’s impact with a conducting surface of an electrode are reported in literature.<sup>1,2</sup> For instance, Compton reported the observation of micrometer-sized particle collision events with an electrode surface by measuring non-faradaic charge transfer due to a change in the substrate electrode double-layer capacitance<sup>1</sup> or due to the individual charging current flows<sup>2</sup> during the particle’s impact with the electrode. Recently, electrochemical approaches for detecting a single NP by measuring faradaic charge transfer during its impact with the electrode have also been reported by other groups.<sup>3–12</sup> For example, single NPs can be detected by measuring charge transfer due to the electrodisolution of single NPs,<sup>3,4</sup> underpotential deposition of metal on a single-metal NP,<sup>5,6</sup> and electroreduction of redox-active ligands immobilized on the metal NP<sup>7</sup> when NP

encounters the electrode. Bard and co-workers developed an electrochemical method termed “electrocatalytic amplification” for detecting single-NP collision events based on the measurement of electrocatalytic current due to the electrochemical processes (oxidation and/or reduction of the species present in solution) occurring on the surface of the NP whenever a NP collides with an inert ultramicroelectrode (UME) (gold, platinum, platinum oxide, and carbon), which otherwise cannot catalyze the reaction.<sup>8–12</sup> Compared to that in other methods, the catalytic signal is greatly amplified in this approach because of the continued electron flow associated with the redox reaction. Hence, among all the electrochemical methods for detecting a single NP described above, methods based on electrocatalytic amplification offer the greatest improvement in measurement time response and detection sensitivity.

Polarography has been used for studying the properties of colloidal particles such as titanium oxide and mixed titanium oxide/iron oxide particles.<sup>13,14</sup> Recently, our group reported the advantages of utilizing a Hg/Pt UME as an electrode platform for detecting and screening Pt NP sizes through electrocatalytic amplification using hydrazine oxidation as the redox indicator

Received: July 24, 2013

Revised: October 3, 2013

Published: November 4, 2013

reaction.<sup>15</sup> Figure 1 shows the schematic representation of this principle involved in detecting single-Pt NPs through electro-

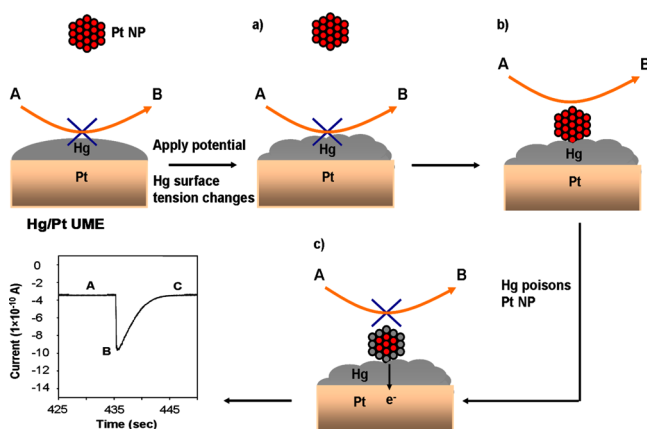


**Figure 1.** Schematic representation of the principle involved in single-Pt NP detection via collision at a Hg/Pt UME and the current enhancement by an electrocatalytic reaction.

catalytic amplification at Hg/Pt UMEs with hydrazine oxidation. Here, the Hg/Pt UME is held at a potential where catalytic reaction does not occur at the surface of the Hg/Pt UME. However, when a Pt NP either collides with the Hg/Pt UME or is at a distance at which electrons can tunnel between the Hg/Pt UME and the Pt NP, there is an increase in current due to the electrocatalytic oxidation of the species on the surface of the Pt NP. Once the Pt NP contacts the Hg/Pt UME, Hg poisons the Pt NP (due to amalgamation)<sup>16</sup> and turns off the catalytic reaction, resulting in a decrease in current that eventually decays to the background level. Hence, utilization of a Hg/Pt UME as an electrode material for detecting a single-Pt NP led to the observation of a “spike”-shaped (reversible)  $i-t$  response when the Pt NP contacted the electrode, in contrast to the observation of a stepwise “staircase” (irreversible)  $i-t$  response for Pt NP collisions at Au UMEs where the Pt NP sticks and retains its catalytic activity. In addition to observing a reversible  $i-t$  response, we observed higher signal-to-noise (S/N) ratios at Hg/Pt UMEs that allow more precise quantitative analysis than that previously observed at carbon or Au UMEs.<sup>15</sup> Also, there is a reduction in the extent of electrode fouling processes at Hg/Pt UMEs, making them reusable for sequential detection of different NP samples. Here, we describe the influence of the redox indicator reaction (proton reduction vs hydrazine oxidation at a Hg/Pt UME) and the electrode material (Hg vs Bi) on the  $i-t$  response during single-Pt NP collisions with the electrode. Apart from aiding in gaining an improved understanding of the factors that influence the  $i-t$  response during single-NP collision events at Hg/Pt and Bi/Pt UMEs, this work is important for several other reasons. (i) Proton reduction studies are performed in a phosphate buffer solution eliminating the use of hydrazine that is reported to induce Pt NP aggregation and complicate single-NP studies,<sup>17</sup> and (ii) because single-Pt NP collision events are detected in phosphate buffer at neutral pH, this method has great potential for application in detecting individual DNA hybridization events for immunoassays.<sup>18</sup>

## EXPERIMENTAL METHODS

Citrate-capped Pt NPs were synthesized using the procedure reported previously.<sup>19</sup> Briefly, 7.8 mL of a 0.2% chloroplatinic acid hydrate solution was added to 100 mL of boiling nanopure water. After this solution had been boiled for 1 min, 2.4 mL of a solution containing 1% sodium citrate and 0.05% citric acid was added. This solution was allowed to boil for 0.5 min. Finally, 1.2 mL of a freshly prepared solution containing 0.08% sodium borohydride, 1% sodium citrate, and 0.05% citric acid was added, and the solution was boiled for an additional 10 min. The solution was then allowed to cool to room temperature. The product was dialyzed to remove excess salt prior to its use. The Pt NP concentration was determined by dividing the Pt metal ion concentration by the number of Pt atoms per Pt NP. The Pt metal ion concentration was estimated using the UV-vis method reported previously.<sup>15</sup> The number of Pt atoms in a NP was estimated via transmission electron microscopy (TEM).<sup>15</sup>

The Pt UME was modified with Hg and Bi following the procedures reported in the literature.<sup>20,21</sup> Hg was electrodeposited on a Pt UME from a solution containing 5.7 mM mercury nitrate in 0.5% concentrated HNO<sub>3</sub> in 1 M KNO<sub>3</sub> in chronocoulometric mode by holding the potential at 0.1 V versus Ag/AgCl for 333 s.<sup>20</sup> Bi was electrodeposited on the Pt UME from a solution containing 0.02 M BiO<sup>+</sup> in 2 M HClO<sub>4</sub> in chronocoulometric mode by holding the potential at 0.14 V versus Ag/AgCl until  $\sim 1.2 \times 10^{-4}$  C of Bi was deposited.<sup>21</sup> Successful modification of the Pt UME surface with Hg and Bi was confirmed by testing the onset potential for the H<sub>2</sub> evolution reaction at the Pt UME before and after electrodepositing Hg and Bi (see Figure S1 of the Supporting Information).

## RESULTS AND DISCUSSION

As shown in Figure 2, proton reduction is sluggish at a Hg/Pt UME in 50 mM phosphate buffer (pH  $\sim 4.0$ ) at potentials ( $E$ ) greater than of  $-0.9$  V versus Ag/AgCl. However, at a pure Pt UME, the steady state diffusion-limited current is seen at potentials ( $E$ ) of less than or equal to  $-0.9$  V. Panels B and C of Figure 2 show  $i-t$  plots recorded at a Hg/Pt UME at a potential of  $-0.9$  V before and after injecting 6 pM Pt NPs in a 50 mM phosphate buffer solution (pH  $\sim 4.0$ ). The  $i-t$  response before injecting Pt NPs into the phosphate buffer solution or the background current is essentially constant at  $5.4 \times 10^{-10}$  A (Figure 2B) and decays very slowly over time. As seen in Figure 2C, after Pt NPs had been injected into a phosphate buffer solution (pH  $\sim 4.0$ ), very distinct current spikes are observed at the Hg/Pt UME. No current events were observed at the Hg/Pt UME even when the  $i-t$  response was recorded for an extended period of time (1000 s) at the Hg/Pt UME in a 50 mM phosphate buffer solution (pH  $\sim 4.0$ ) in the absence of Pt NPs (Figure S2 of the Supporting Information). These data suggest that the current spikes observed after injecting Pt NPs into a phosphate buffer solution are due to proton reduction occurring on the surface of the Pt NPs during the collision with the electrode surface. We previously reported the observation of spike-shaped  $i-t$  response for hydrazine oxidation with citrate-capped Pt NPs at a Hg/Pt UME due to the deactivation of Pt NP as Hg poisons the catalytic activity of Pt NP due to amalgamation.<sup>15</sup> However, the current spikes observed for proton reduction are distinctly different from the current spikes observed for hydrazine oxidation with citrate-capped Pt NPs at a Hg/Pt UME. The current spike due to proton reduction at the Hg/Pt UME shows a very rapid increase and a very fast decay in current to the background level. In the case of hydrazine oxidation, the current spike shows a very fast increase but a much slower decay of current to the background level. In the current spike response, the current decays to the background level in 0.7–4 ms for proton reduction and 2–5

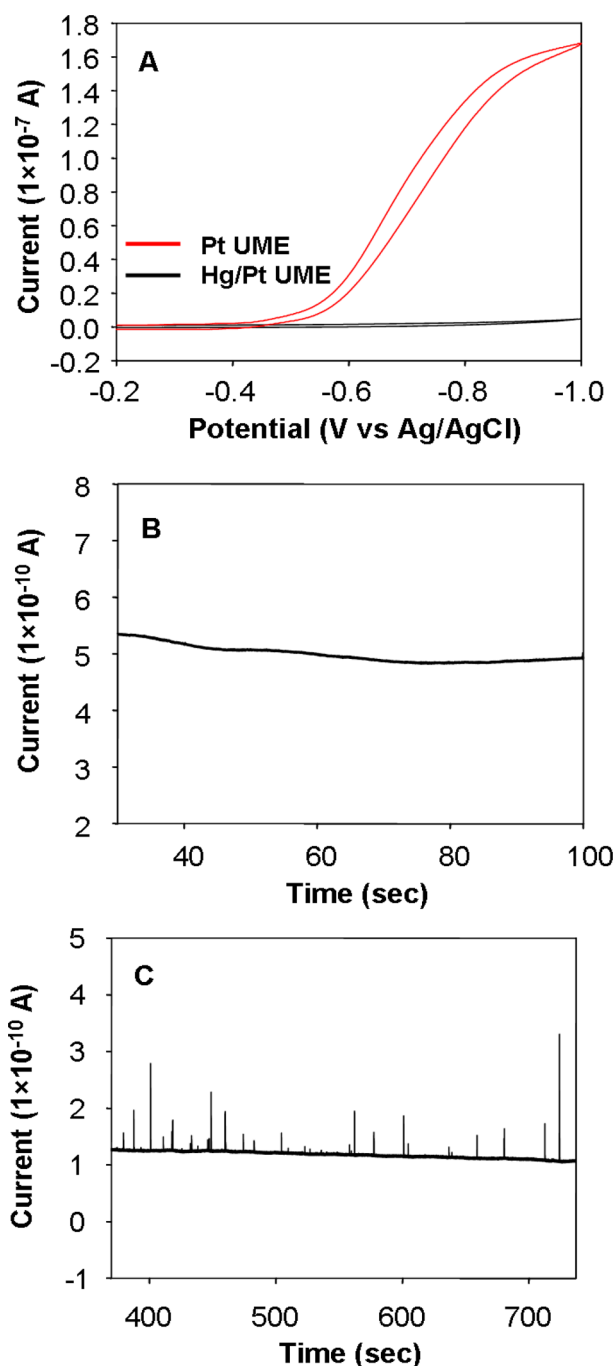


**Figure 2.** (A) Cyclic voltammogram of proton reduction in 50 mM phosphate buffer (pH  $\sim 4.0$ ): red for the Pt UME and black for the Hg/Pt UME (radius of  $12.5 \mu\text{m}$ ). (B and C) Chronoamperometric plots recorded at the Hg/Pt UME in 50 mM phosphate buffer (pH  $\sim 4.0$ ) before (B) and after (C) injecting Pt NPs [applied potential ( $V_{\text{app}}$ ),  $-0.9 \text{ V}$  vs Ag/AgCl; data acquisition interval ( $t_{\text{data}}$ ),  $1.5 \text{ ms}$ ; NP size,  $\sim 4.5 \text{ nm}$ ; NP concentration,  $\sim 6 \text{ pM}$ ].

s for hydrazine oxidation. Hence, as shown in Figure 3, current spikes due to proton reduction with Pt NPs are sharper than current spikes due to hydrazine oxidation at a Hg/Pt UME. This could be due to either the difference in the pH of the phosphate buffer (pH  $\sim 4$  for proton reduction and pH  $\sim 7.5$  for hydrazine oxidation) or the applied potential ( $-0.9 \text{ V}$  for proton reduction and  $-0.05 \text{ V}$  vs Ag/AgCl for hydrazine oxidation). Pt NPs used in this study are stabilized with citrate,

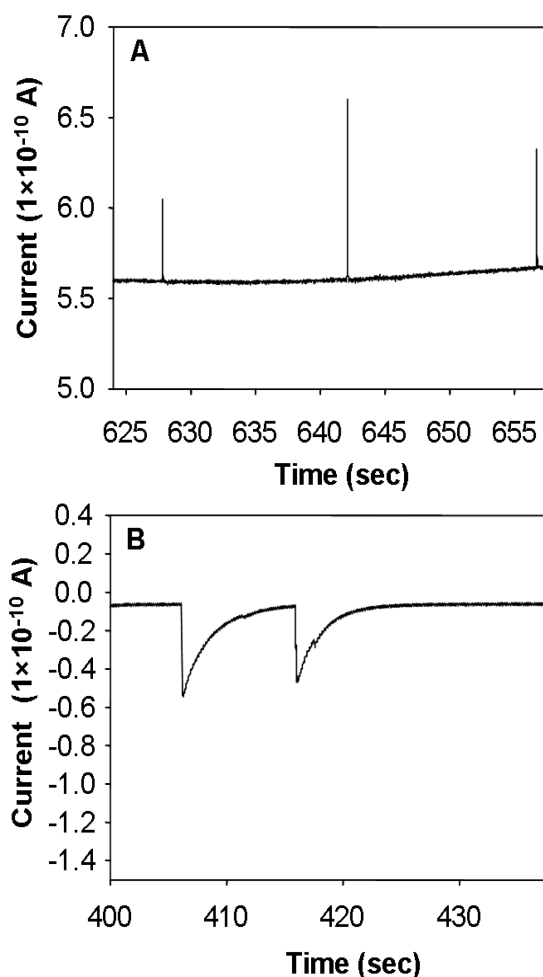


**Figure 3.** Chronoamperometric plot recorded at a Hg/Pt UME after injecting Pt NPs (A) in 50 mM phosphate buffer (pH  $\sim 4.0$ ) for proton reduction and (B) in 15 mM hydrazine in 50 mM phosphate buffer (pH  $\sim 7.0$ ) for hydrazine oxidation [applied potential ( $V_{\text{app}}$ ),  $-0.9 \text{ V}$  vs Ag/AgCl; data acquisition interval ( $t_{\text{data}}$ ),  $1.5 \text{ ms}$ ; NP size,  $\sim 4.5 \text{ nm}$ ; NP concentration,  $\sim 6 \text{ pM}$ ].

and in a low-pH (high- $\text{H}^+$  concentration) solution, protonation of the carboxylate groups of the stabilizing citrate can make the Pt NPs unstable. This could lead to the deactivation of Pt NPs (amalgamation) at a faster rate, resulting in sharp current spikes in the case of proton reduction. To determine the effect of pH on the  $i-t$  response, both proton reduction and hydrazine oxidation experiments were performed in solutions at neutral pH (pH  $\sim 7.0$ ). Figure 4 shows the  $i-t$  response at a Hg/Pt UME for proton reduction after injecting Pt NPs in phosphate buffer (pH  $\sim 7.0$ ). Current spikes due to proton reduction with Pt NPs in pH  $\sim 7.0$  phosphate buffer are similar to current spikes due to proton reduction in pH  $\sim 4.0$  phosphate buffer. In a current spike due to proton reduction with Pt NPs, the current decayed to the background level in  $0.8\text{--}2 \text{ ms}$  in pH  $\sim 7.0$  phosphate buffer and  $0.7\text{--}4 \text{ ms}$  in pH  $\sim 4.0$  phosphate buffer. Hence, as shown in Figure 4, current spikes due to proton reduction are sharper than current spikes due to hydrazine oxidation at pH  $\sim 7.0$ , as well. This suggests that the difference in the  $i-t$  response for proton reduction and hydrazine oxidation is not due to the difference in pH but is more likely due to the applied potential. In the case of proton reduction, a Hg/Pt UME is held at a more negative potential ( $-0.9 \text{ V}$ ) compared to that of hydrazine oxidation ( $-0.05 \text{ V}$  vs Ag/

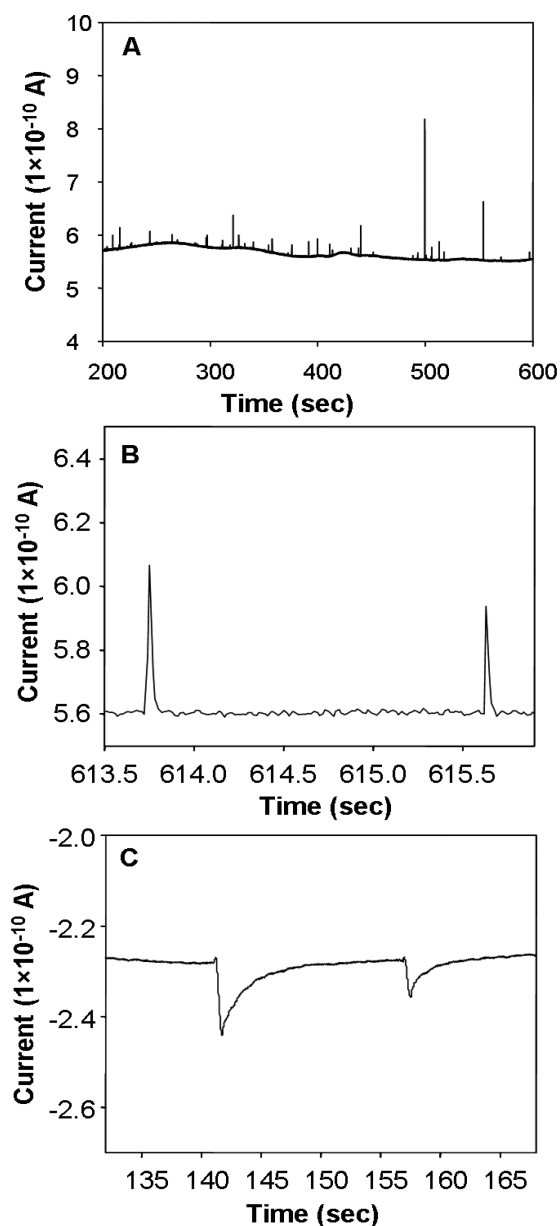


**Figure 4.** (A) Chronoamperometric plot recorded at a Hg/Pt UME after injecting Pt NPs in (A) 50 mM phosphate buffer (pH  $\sim$ 7.0) for proton reduction and (C) 15 mM hydrazine in 50 mM phosphate buffer. (B) Close-up of a portion of the  $i$ - $t$  plot shown in panel A. The solution pH was adjusted to  $\sim$ 7.0 [applied potential ( $V_{app}$ ),  $-0.9$  V vs Ag/AgCl; data acquisition interval ( $t_{data}$ ), 1.5 ms; NP size,  $\sim$ 4.4 nm; NP concentration,  $\sim$ 6 pM].

AgCl). Thus, at a more negative potential ( $-0.9$  V), the Pt NPs either do not stick to the Hg/Pt UME or are deactivated at a faster rate, resulting in sharp current spikes for proton reduction. Citrate-capped Pt NPs have a negative surface charge at neutral pH. Hence, at more at negative potentials ( $-0.9$  V), Pt NPs might not stick to the Hg/Pt UME but rather “bounce” back into the solution due to electrostatic repulsion. Bard and co-workers previously reported the observation of a spike-shaped  $i$ - $t$  response in the case of water oxidation with  $IrO_x$  NPs at a Au UME and suggested that the NP bounces off the electrode rather than remaining stuck on the electrode surface.<sup>10</sup> Assuming that the sharp current spikes due to proton reduction with citrate-capped Pt NPs at Hg/Pt UME are due to

electrostatic repulsion and are not specific to Hg, one would expect to observe a similar  $i$ - $t$  response under similar conditions with a different electrode material such as Bi. To test this hypothesis, proton reduction experiments were performed at Bi/Pt UMEs with the same citrate-capped Pt NPs. Bi was chosen because proton reduction is also sluggish at Bi electrodes (Figure 5A). Hence, by employing Bi/Pt UME as an electrode material, single-Pt NP collision experiments utilizing proton reduction as a redox indicator reaction can be performed under the same experimental conditions as in the

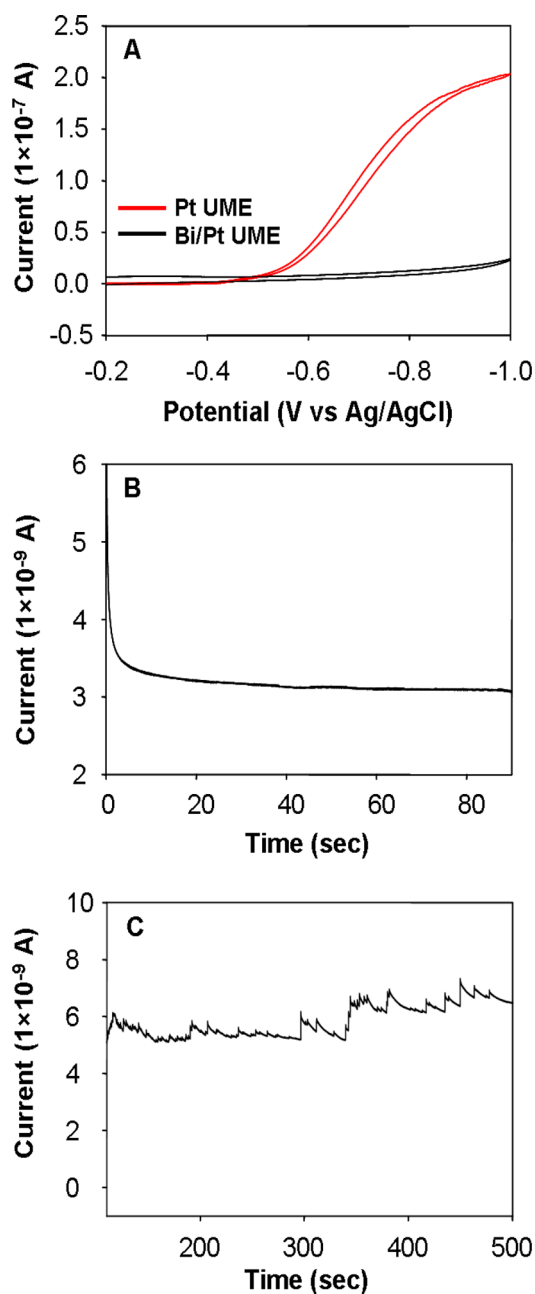


**Figure 5.** (A) Cyclic voltammogram of proton reduction in 50 mM phosphate buffer (pH  $\sim$ 4.0): red for the Pt UME and black for the Bi/Pt UME (radius of 12.5  $\mu$ m). (B and C) Chronoamperometric plot recorded at the Bi/Pt UME in 50 mM phosphate buffer (pH  $\sim$ 4.0) before (B) and after (C) injecting Pt NPs [applied potential ( $V_{app}$ ),  $-0.9$  V vs Ag/AgCl; data acquisition interval ( $t_{data}$ ), 1.5 ms; NP size,  $\sim$ 4.5 nm; NP concentration,  $\sim$ 6 pM].

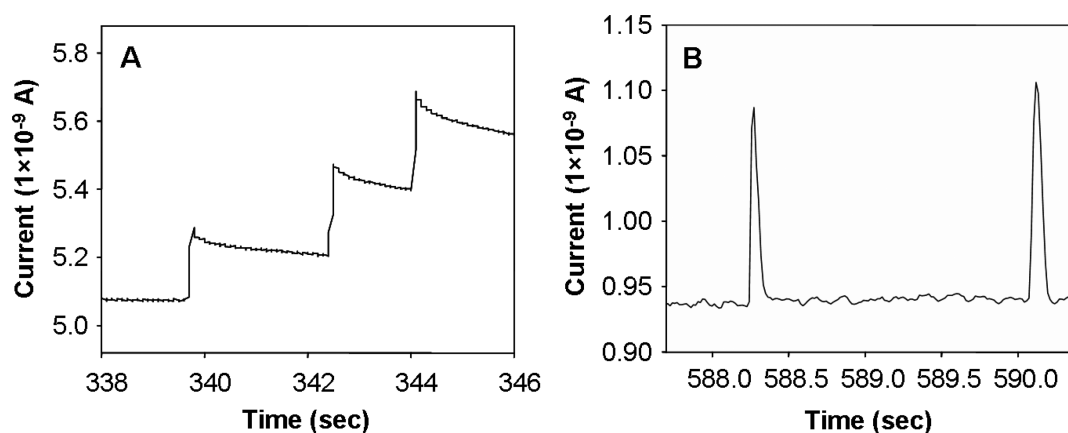


**Figure 6.** Chronoamperometric plot recorded after injecting Pt NPs in 50 mM phosphate buffer (pH  $\sim$ 4.0) at (A) the Bi/Pt UME and (B) the Hg/Pt UME [applied potential ( $V_{app}$ ),  $-0.9$  V vs Ag/AgCl; data acquisition interval ( $t_{data}$ ), 1.5 ms; NP size,  $\sim$ 4.5 nm; NP concentration,  $\sim$ 6 pM].

case of the Hg/Pt UME (at potentials more negative than  $-0.9$  V vs Ag/AgCl).

Panels B and C of Figure 5 show  $i-t$  plots recorded at the Bi/Pt UME at a potential of  $-0.9$  V before and after injecting 6 pM Pt NPs in a 50 mM phosphate buffer solution (pH  $\sim$ 4.0). The background current was  $3.5 \times 10^{-9}$  A (Figure 5B) and is 1 order of magnitude higher than the background current observed at the Hg/Pt UME under similar conditions, possibly because of the presence of pits or defects in the Bi film. The background current remained essentially constant, decaying very slowly over the time course of the experiment (Figure S3 of the Supporting Information). As shown in Figure 5C, after injection of 6 pM Pt NPs in a phosphate buffer solution (pH  $\sim$ 4.0), the current increased and exhibited a stepwise (staircase) response. Very distinct current steps were observed at the Bi/Pt UME due to proton reduction with Pt NPs as opposed to the current spikes at a Hg/Pt UME under similar experimental conditions. The staircase  $i-t$  response suggests that the Pt NP sticks to the Bi/Pt UME upon contact and retains its catalytic activity because further collisions contribute to the buildup of the overall increase in current.<sup>8</sup> A similar staircase  $i-t$  response was observed at the Bi/Pt UME in pH  $\sim$ 7.0 phosphate buffer, as well (Figure S4 of the Supporting Information). This indicates that the citrate-capped Pt NPs do stick to the electrode at  $-0.9$  V and the sharp current spikes observed at Hg/Pt UME for proton reduction are not due to electrostatic repulsion but are due to the deactivation of Pt NPs at a faster rate at  $-0.9$  V for proton reduction. We also note that closer analysis of current transients at the Bi/Pt UMEs reveals that the current decays approximately 10–40% in 2 s following a collision (Figure 6A). The difference in current response is small even at long polarization times at Bi/Pt UMEs. This suggests that the current decay is mainly due to the progressive surface contamination of Pt NPs. This could be due to the adsorption of hydrogen atoms into the lattice of the Pt NPs. Pletcher suggested this as a possible cause for the deactivation of Pt UMEs in a previous report.<sup>22</sup> Also, electrogeneration of hydrogen bubbles due to proton reduction at the electrode surface is reported in the literature.<sup>23</sup> This could also be one of the possible reasons for the observed current decay following a collision event at Bi/Pt UMEs. The hydrogen bubble generated at the electrode surface might hinder Pt NP's contact with the electrode. As a result, Pt NP might not experience the total potential that is applied to the electrode because of which Pt NP might not be capable of

catalyzing the reaction as it would if it were in good contact with the electrode surface. This probably could result in current decay following a collision event. In the case of proton reduction, as the applied potential is more negative the inner Helmholtz plane might contain more cations compared to the situation for hydrazine oxidation. This might affect the interaction of the Pt NP with the electrode, which might in turn affect the shape of the  $i-t$  response during single-Pt NP collisions with the UME. However, the current decay in a current spike due to proton reduction with Pt NPs at Hg/Pt UMEs cannot be due to only the influence of double-layer structure, surface contamination of the Pt NP (due to hydrogen adsorption), or generation of a hydrogen bubble that hinders Pt NP's contact with the electrode as the current decays to the background level in only a few milliseconds (Figure 6B). Rather, the response is heavily influenced by the applied potential in the case of Hg as surface tension (electrocapillarity) is known to significantly change as a function of applied potential. Specifically, the surface tension of Hg increases and decreases with potential and is maximal at the potential of zero charge (PZC).<sup>24</sup> As the applied potential deviates from the PZC, the surface tension decreases and the PZC of Hg in a neutral solution is reported to be in the range of  $-0.5$  V versus the sodium-saturated calomel electrode (SSCE).<sup>25</sup> Also, the Hg beating heart phenomenon in neutral and basic solutions solely due to the electrocapillary effect has also been reported in the literature, and the potential was determined to be in the range of  $-1.0$  to  $-1.5$  V versus SSCE during Hg drop oscillations.<sup>25</sup> On the basis of all the findings mentioned above from the literature, we propose that as the surface tension of Hg is lower at  $-0.9$  V, Pt NPs might sink more easily and quickly into Hg, resulting in faster  $i-t$  decay for proton reduction compared to hydrazine oxidation ( $-0.05$  V) at Hg/Pt UMEs.

The collision frequency and the average size of Pt NPs were estimated from  $i-t$  responses recorded at both Hg/Pt UME and Bi/Pt UMEs for proton reduction in pH  $\sim$ 4.0 phosphate buffer. At both Hg/Pt and Bi/Pt UMEs, the number of collisions increases with an increase in Pt NP concentration and the collision frequency scales linearly with concentration (see Figures S5 and S6 of the Supporting Information) as has been reported previously.<sup>9,15</sup> However, the collision frequency estimated from the  $i-t$  responses recorded at a Hg/Pt UME ( $0.001$ – $0.003$  pM $^{-1}$  s $^{-1}$ ) for proton reduction with Pt NPs is lower than the value reported in the literature for hydrazine oxidation at a Hg/Pt UME<sup>15</sup> ( $0.016$ – $0.024$  pM $^{-1}$  s $^{-1}$ ) and a Au

UME ( $0.012\text{--}0.020\text{ pM}^{-1}\text{ s}^{-1}$ ).<sup>9</sup> This difference could be due to the effect of the instrumental response such as the sampling time interval on the acquired  $i\text{--}t$  response. In 68% of the current spikes due to proton reduction with Pt NPs at Hg/Pt UMEs, the current decayed to the background level in  $<1$  ms, whereas a sampling interval of 1.5 ms is used in the experiments. This time scale indicates that NP deactivation or amalgamation is faster than the sampling time interval. Hence, the potentiostat might not record all the collision events, resulting in a lower measured collision frequency for proton reduction at Hg/Pt UMEs, whereas the collision frequency obtained at a Bi/Pt UME ( $0.009\text{--}0.026\text{ pM}^{-1}\text{ s}^{-1}$ ) for proton reduction with Pt NPs is in good agreement with the literature value, indicating that the applied potential at Bi does not influence the sticking probability of the Pt NPs.

The Pt NP size distribution from the distribution of peak currents was also determined using the equation reported for calculating the amplitude of the current “step” at the mass transfer-limited current generated at individual spherical metal NPs in contact with a planar electrode.<sup>9</sup>

$$I = 4\pi(\ln 2)nFDCr$$

where  $I$  is the amplitude of the current,  $n$  is the number of electrons,  $F$  is Faraday’s constant,  $D$  is the diffusion coefficient of reactants at concentration  $C$ , and  $r$  is the radius of the single-metal NP. At Bi/Pt UMEs, the current step amplitude was concentrated over a range of 50–190 pA. As shown in Figure S7 of the Supporting Information, the average size determined from the  $i\text{--}t$  plot ( $3.9 \pm 1.7$  nm) correlated well with theory and the TEM-derived average size ( $4.5 \pm 2.0$  nm). We note that though the equation used for estimating the NP size does not account for the current decay over time we still observe a good correlation between the size distributions determined from the  $i\text{--}t$  transients due to hydrazine oxidation at Hg/Pt UMEs and TEM-derived size distributions.<sup>15</sup> Hence, on the basis of the same assumptions that the integrated charge passed per spike during a single collision event is equal to the current step amplitude, we can estimate the NP size from the  $i\text{--}t$  profiles due to proton reduction at Hg/Pt UMEs. The integrated charge passed per spike during single-Pt NP collision concentrated over a range of 30–80 pC at Hg/Pt UMEs (Figure S7 of the Supporting Information), corresponding to an average size of  $1.5 \pm 0.6$  nm, which is smaller than the TEM-derived average size. This discrepancy could be due to the influence of sampling interval on the measured  $i\text{--}t$  response. Because the NP deactivation or amalgamation process is faster than the sampling interval, the initial peak-to-peak amplitude that significantly affects the charge integral may not always represent the actual proton reduction response occurring on the surface of the pristine Pt NP during its impact with the Hg/Pt UME. Rather, the response could result from the collision of a partly poisoned Pt NP that would yield an overall lower initial peak-to-peak amplitude and therefore the estimation of a smaller average size. The average integrated charge passed per current spike at Hg/Pt UMEs and the current step amplitude at Bi/Pt UMEs due to proton reduction in pH  $\sim 7.0$  phosphate buffer with Pt NPs are greater than estimated values based on theory. The overall integrated charge passed per spike at Hg/Pt UMEs and the current step amplitude at Bi/Pt UMEs increased with an increase in proton concentration but did not scale linearly with concentration. We also note that because the NP sizes determined from  $i\text{--}t$  profiles at a Hg/Pt UME for proton reduction did not correlate with the theory or the TEM-derived

NP sizes, we estimated the percentage of current transients due to aggregates form  $i\text{--}t$  profiles due to proton reduction at Bi/Pt UMEs. Fewer current transients (13%) are observed due to aggregates for proton reduction at Bi/Pt UMEs than for hydrazine oxidation (32%) at Hg/Pt UMEs, again supporting the hypothesis that hydrazine oxidation induces aggregation of Pt NPs during their detection.<sup>17</sup> We note that to reinforce our conclusion that surface tension influences the amalgamation process that in turn affects the  $i\text{--}t$  response during single-Pt NP collisions with the Hg/Pt UME, we performed collision experiments at Hg/Pt UMEs for proton reduction with Pt NPs at different applied potentials (more negative than PZC and less negative than  $-0.9$  V vs Ag/AgCl). We did not observe any significant difference in the shape of the  $i\text{--}t$  response with a change in the applied potential (see Figure S8 of the Supporting Information). This could also be due to the influence of the sampling interval on the  $i\text{--}t$  response. We used the lowest possible sampling interval of which our potentiostat is capable, but because amalgamation is faster than the sampling interval, we might not have observed any difference in the  $i\text{--}t$  response as a function of applied potential.

## CONCLUSIONS

In summary, our results demonstrate that the applied potential has a significant influence on the  $i\text{--}t$  response observed for single-Pt NP collision events at Hg/Pt UMEs. The applied potential affects the surface tension of Hg that in turn affects the rate of deactivation of Pt NPs (amalgamation) or the rate at which the current decays to the background level in a current spike at the Hg/Pt UME due to single-Pt NP collisions. Also, the observation of a stepwise staircase  $i\text{--}t$  response for proton reduction with Pt NPs at Bi/Pt UMEs in contrast to the spike-shaped  $i\text{--}t$  responses at Hg/Pt UMEs under similar conditions indicates that the electrode material plays an important role in influencing the shape of the  $i\text{--}t$  response. This work continues the development of Hg/Pt UMEs as a reliable and robust electroanalytical tool for screening the catalytic activity of a single NP through electrocatalytic amplification.

## ASSOCIATED CONTENT

### Supporting Information

Current–time plots for proton reduction at different pHs, in the absence of Pt NPs for extended sampling times at Hg/Pt UMEs and Bi/Pt UMEs, and TEMs and histograms showing Pt NP size distributions. This material is available free of charge via the Internet at <http://pubs.acs.org>.

## AUTHOR INFORMATION

### Corresponding Author

\*E-mail: [stevenson@mail.utexas.edu](mailto:stevenson@mail.utexas.edu). Telephone: (512) 232-9160. Fax: (512) 471-8696.

### Notes

The authors declare no competing financial interest.

## ACKNOWLEDGMENTS

We thank the DTRA (Grant HDTRA1-11-1-0005) for financial support and Dr. Allen J. Bard, Dr. Richard M. Crooks, and Dr. Bo Zhang for valuable discussions. R.D. acknowledges Nellymar Membreno for acquiring TEM images.

## REFERENCES

- (1) Rees, N. V.; Banks, C. E.; Compton, R. G. Ultrafast chronoamperometry of acoustically agitated solid particulate suspensions: Nonfaradaic and faradaic processes at a polycrystalline gold electrode. *J. Phys. Chem. B* **2004**, *108*, 18391–18394.
- (2) Clegg, A. D.; Rees, N. V.; Banks, C. E.; Compton, R. G. Ultrafast chronoamperometry of single impact events in acoustically agitated solid particulate suspensions. *ChemPhysChem* **2006**, *7*, 807–811.
- (3) Zhou, Y.-G.; Rees, N. V.; Compton, R. G. The electrochemical detection and characterization of silver nanoparticles in aqueous solution. *Angew. Chem., Int. Ed.* **2011**, *50*, 4219–4221.
- (4) Zhou, Y.-G.; Rees, N. V.; Pillay, J.; Tshikhudo, R.; Vilakazi, S.; Compton, R. G. Gold nanoparticles show electroactivity: Counting and sorting nanoparticles upon impact with electrodes. *Chem. Commun.* **2012**, *48*, 224–226.
- (5) Rees, N. V.; Zhou, Y.-G.; Compton, R. G. Nanoparticle–electrode collision processes: The underpotential deposition of thallium on silver nanoparticles in aqueous solution. *ChemPhysChem* **2011**, *12*, 2085–2087.
- (6) Zhou, Y.-G.; Rees, N. V.; Compton, R. G. Nanoparticle–electrode collision processes: The electroplating of bulk cadmium on impacting silver nanoparticles. *Chem. Phys. Lett.* **2011**, *511*, 183–186.
- (7) Zhou, Y.-G.; Rees, N. V.; Compton, R. G. The electrochemical detection of tagged nanoparticles via particle–electrode collisions: Nanoelectroanalysis beyond immobilisation. *Chem. Commun.* **2012**, *48*, 2510–2512.
- (8) Xiao, X.; Bard, A. J. Observing single nanoparticle collisions at an ultramicroelectrode by electrocatalytic amplification. *J. Am. Chem. Soc.* **2007**, *129*, 9610–9612.
- (9) Xiao, X.; Fan, F.-R. F.; Zhou, J.; Bard, A. J. Current transients in single nanoparticle collision events. *J. Am. Chem. Soc.* **2008**, *130*, 16669–16677.
- (10) Zhou, H.; Park, J. H.; Fan, F.-R. F.; Bard, A. J. Observation of single metal nanoparticle collisions by open circuit (mixed) potential changes at an ultramicroelectrode. *J. Am. Chem. Soc.* **2012**, *134*, 13212–13215.
- (11) Kwon, S. J.; Zhou, H.; Bard, A. J. Electrochemistry of single nanoparticles via electrocatalytic amplification. *Isr. J. Chem.* **2010**, *50*, 267–276.
- (12) Kwon, S. J.; Fan, F.-R. F.; Bard, A. J. Observing iridium oxide (IrO<sub>x</sub>) single nanoparticle collisions at ultramicroelectrodes. *J. Am. Chem. Soc.* **2010**, *132*, 13165–13167.
- (13) Heyrovský, M.; Jirkovsky, J.; Struplova-Bartackova, M. Polarography and voltammetry of aqueous TiO<sub>2</sub> colloidal solutions. *Langmuir* **1995**, *11*, 4300–4308.
- (14) Heyrovský, M.; Jirkovsky, J.; Struplova-Bartackova, M. Polarography and voltammetry of mixed titanium(IV) oxide/iron(III) oxide colloids. *Langmuir* **1995**, *11*, 4309–4312.
- (15) Dasari, R.; Robinson, D. A.; Stevenson, K. J. Ultrasensitive electroanalytical tool for sizing, detecting and evaluating the catalytic activity of platinum nanoparticles. *J. Am. Chem. Soc.* **2013**, *135*, 570–573.
- (16) Whitesides, G. M.; Hackett, M.; Brainard, R. L.; Lavalleye, J. P. P. M.; Sowinski, A. F.; Izumi, A. N.; Moore, S. S.; Brown, D. W.; Staudt, E. M. Suppression of unwanted heterogeneous platinum(0)-catalyzed reactions by poisoning with mercury(0) in systems involving competing homogeneous reactions of soluble organoplatinum compounds: Thermal decomposition of bis(triethylphosphine)-3,3,4,4-tetramethylplatinacyclopentane. *Organometallics* **1985**, *4*, 1819–1830.
- (17) Kleijn, S. E. F.; Serrano-Bou, B.; Yanson, A. I.; Koper, M. T. M. Influence of hydrazine induced aggregation on the electrochemical detection of platinum nanoparticles. *Langmuir* **2013**, *29*, 2054–2064.
- (18) Alligant, T. M.; Nettleton, E. G.; Crooks, R. M. Electrochemical detection of individual DNA hybridization events. *Lab Chip* **2013**, *13*, 349–354.
- (19) Bigall, N. C.; Härtling, T.; Klose, M.; Simon, P.; Eng, L. M.; Eychmüller, A. Monodisperse platinum nanospheres with adjustable diameters from 10 to 100 nm: Synthesis and distinct optical properties. *Nano Lett.* **2008**, *8*, 4588–4592.
- (20) Wehmeyer, K. R.; Wightman, M. Cyclic voltammetry and anodic stripping voltammetry with mercury ultramicroelectrodes. *Anal. Chem.* **1985**, *57*, 1989–1993.
- (21) Vereecken, P. M.; Rodbell, K.; Ji, C.; Searson, P. C. Electrodeposition of bismuth thin films on n-GaAs (110). *Appl. Phys. Lett.* **2005**, *86*, 121916–121919.
- (22) Pletcher, D. In *Microelectrodes: Theory and Application*; Montenegro, M. I., Queiros, M. A., Daschbach, J. L., Eds.; Kluwer Academic: Dordrecht, The Netherlands, 1991; p 472.
- (23) Luo, L.; White, H. S. Electrogeneration of single nanobubbles at sub-50-nm-radius platinum nanoelectrodes. *Langmuir* **2013**, *29*, 11169–11175.
- (24) Grahame, C. D. The electrical double layer and the theory of electrocapillarity. *Chem. Rev.* **1947**, *41*, 441–454.
- (25) Olson, J.; Ursenbach, C.; Birss, V. I.; Laidlaw, W. G. Hydrodynamic mode selection due to the electrocapillary effect: The mercury beating heart in neutral and basic solutions. *J. Phys. Chem.* **1989**, *93*, 8258–8263.